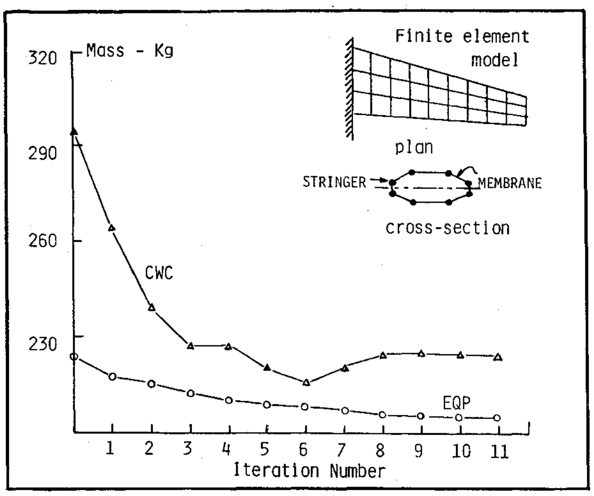

Fig. 1 Objective function convergence histories for both conserative worst-case strategy (CWC) and method, using the equal probability criterion (EQP).

represent the structural deformation for the cantilevered wing. Addition of rigid-body modes in plunge and pitch presents no additional difficulty. A 2.54 m/s (typical of storm conditions) intensity, Dryden gust spectrum, was selected for the input load.

In the first example, cross-sectional areas of bar elements were selected as the design varibles. An allowable stress of 1761.4 kg/cm^2 and values of $L_s w = L_F = 17{,}250$ h were used in the optimum design process. The first bending mode dominated the stress distribution as evidenced by a concentration of material at the root, and the first excursion constraint was active at the optimum. Both finite-difference and semi-analytical gradient computations were used with essentially similar results.

A second set of numerical results reported here pertains to the implementation and verification of constraints based on an equal-probability-of-load-combination criterion. This problem involved a combination of deterministic static loads and gust-induced random loads. The thickness of six sets of panel members was altered during redesign. A $p(x,y)$ value of 0.99 was selected for the equal probability criterion. An allowable stress magnitude of 2465.9 kg/cm^2 was specified, and a total of 40 load combinations were chosen to represent the ellipse of equal probability. Optimum designs were obtained on the basis of a worst-case estimate of the stress function given by Eq. (4) and the use of Eq. (3) with values of σ_1 and σ_2 obtained from an equal probability criterion. As shown in Fig. 1, the final optimum weight of the equal-probability-of-load-combination method was 8% less than that obtained from a conservative worst-case strategy. Additional results and a detailed description of the model are presented in Ref. 6.

Concluding Remarks

The principal goal of this study was to develop an optimization capability to design airframe structures for random gust loads in addition to static or dynamic deterministic loads. The combination of optimization algorithms with analysis tools such as EAL and ISAC makes available a tool for stress, displacement, frequency, flutter, and gust-response-constrained optimization. Furthermore, implementation of semi-analytical gradient calculations provides added computational efficiency to the programming system. This system also provides a natural test bed for continuing studies in a multilevel decomposition approach for aeroservoelastic synthesis. The use of an equal-probability-of-load-combination criterion for structural reliability constraints has also been demonstrated for representative structural models.

Acknowledgment

Research support from NASA Langley Research Center under Grant NAG 1-688 is gratefully acknowledged.

References

[1]Hajela, P., "Comments on Gust Response Constrained Optimization," NASA CP-2327, Vol. 2, April 1984.

[2]Johnson, E. H., "Optimization of Structures Undergoing Harmonic or Stochastic Excitation," SUDAAR 501, Stanford Univ., CA, Aug. 1976.

[3]Hajela, P. and Lamb, A., "Automated Structural Synthesis for Nondeterministic Loads," *Computer Methods in Applied Mechanics and Engineering,* Vol. 57, 1986, pp. 25–36.

[4]Gross, D. W. and Sobieski, J. E., "Application to Aircraft Design of Nonlinear Optimization Methods Which Include Probabilistic Constraints," AIAA Paper 80-0153, Jan. 1980.

[5]Stauffer, W. A. and Hoblitt, F. M., "Loads Determination in the Design of the L-1011," *Journal of Aircraft,* Vol. 10, Aug. 1973, pp. 459–467.

[6]Hajela, P. and Bach, C. T., "Optimum Structural Sizing for Gust Induced Response," *Proceedings of 29th AIAA/ASME/ASCE/AHS/ASC SDM Conference,* AIAA, Washington, DC, 1988.

Interactive Boundary-Layer Calculations of a Transonic Wing Flow

Kalle Kaups*
Douglas Aircraft Company, Long Beach, California

Unmeel Mehta†
NASA Ames Research Center, Moffett Field, California

and

Tuncer Cebeci‡
Douglas Aircraft Company, Long Beach, California

Introduction

THE so-called wing C was designed by NASA and the Lockheed-Georgia Company as one in a series for which it was intended to provide reliable experimental data for the purpose of comparisons with computational efforts. The full potential inviscid transonic wing code FL022, in combination with an optimization routine, was used to configure the wing for highly three-dimensional flow by selecting a large sweep angle and a low aspect ratio combined with supercritical sections and considerable twist. It was intended that the flow remain attached at a design Mach number of 0.85 and lift coefficient of 0.5, which corresponds to a 5 deg of angle of attack. The desired pressure distribution was specified at two spanwise locations and the wing was constructed by linear development between the root and tip.

The purpose of this Note is to present results obtained from interactive solutions of inviscid and boundary-layer equations and to compare them with experimental values. Calculated results were obtained with an Euler code and a transonic

Received July 6, 1988; revision received Aug. 8, 1988.

*Senior Staff Engineer, Aerodynamics Research and Technology Group. Member AIAA.

†Research Scientist. Associate Fellow AIAA.

‡Staff Director, Aerodynamics Research and Technology Group. Fellow AIAA.

potential code to provide solutions of the inviscid flow and were interacted with solutions of two-dimensional boundary-layer equations with a strip-theory approximation. The experiments were performed in the NASA Ames Research Center 6×6 ft transonic/supersonic wind tunnel[1,2] and included pressure distributions at five spanwise stations at a chord Reynolds number of 6.8×10^6 and Mach numbers of 0.70, 0.82, 0.85, and 0.90. Transition was fixed at 4.5% chord on both surfaces.

Calculations and Comparison with Experiment

The interactive boundary-layer approach, based on the strip-theory approach to three-dimensional flow, has been described in Ref. 3 and includes incorporating viscous effects into the inviscid flow through a surface-blowing boundary condition. Two inviscid flow procedures corresponding to a full potential code[4] and an Euler code were used in the calculations. The transonic potential code was used in nonconservative form with a numerical grid of $161 \times 25 \times 33$ mesh points and the Euler code $145 \times 25 \times 31$ mesh points arranged in a C-grid in the streamwise and spanwise directions and, in some cases, with an H-grid in the spanwise direction.

Figure 1 allows comparison of the measured and calculated results at $M_\infty = 0.70$. The interactive calculations with the Euler code and H-grid spanwise and with the full potential code agree well with experimental data, except near the leading edge where the flow is supercritical. As expected, the calculated lift coefficients also agree well with the normal force coefficient $C_N = 0.483$ calculated from the measured pressure distributions. It is evident that calculations with the Euler code and C-grid in both directions reproduce the velocity peaks more accurately, except near the wing tip where the local lift is overpredicted over the whole chord. The results of Fig. 2 correspond to $M_\infty = 0.82$ and show attached flow with shocks. The interactive calculations with the Euler code are closer to the measurements than those with the full potential flow solutions. The C-grid was used in spanwise direction mainly to improve results near the wing tip. However, it is clear that better agreement with experiments has resulted near the shock location and over the whole wing, apart from the wing tip where the lift still tends to be overpredicted and caused the wing lift coefficient to exceed the measured normal force coefficient $C_N = 0.53$. It should be noted that the predicted pressure recovery near the trailing edge at the wing tip differs in all cases from the measured values, indicating a strong decambering effect in the experiment.

Figure 3 shows results at the design condition at which flow visualization has shown the flow in the outer 30% of the span to be separated due to strong shock/boundary-layer interaction. The calculations are in good agreement with experiment, except in the region of the separation bubble, and the corresponding lift coefficient is only slightly lower than the measured value of C_N of 0.54. It is surprising that here the results obtained by interaction with the full potential flow method are in better agreement with those of the Euler method than the results of Fig. 2. The pressure distributions obtained at $M_\infty = 0.9$ and the full potential code are again in reasonable agreement with experiments on the inboard and middle portions of the wing, as shown in Fig. 4. The predictions on the outboard portion of the wing show attached flow, whereas the experiments suggest separation because the predicted shock pressure rise is spread out over a considerable distance. Despite this discrepancy, the predicted lift coefficient is close to the measured normal force coefficient C_N of 0.56.

Similar calculations to those of the previous paragraph were reported in Ref. 5 and made use of a zonal Euler/thin-layer Navier-Stokes (ETLNS) code. They were compared to the measurements referred to previously and to those performed with a smaller model, manufactured to the same design, and tested in the Lockheed Georgia 20×28 in. wind tunnel. They showed good agreement for attached flow, particularly for the smaller model. The two sets of results are, however, different

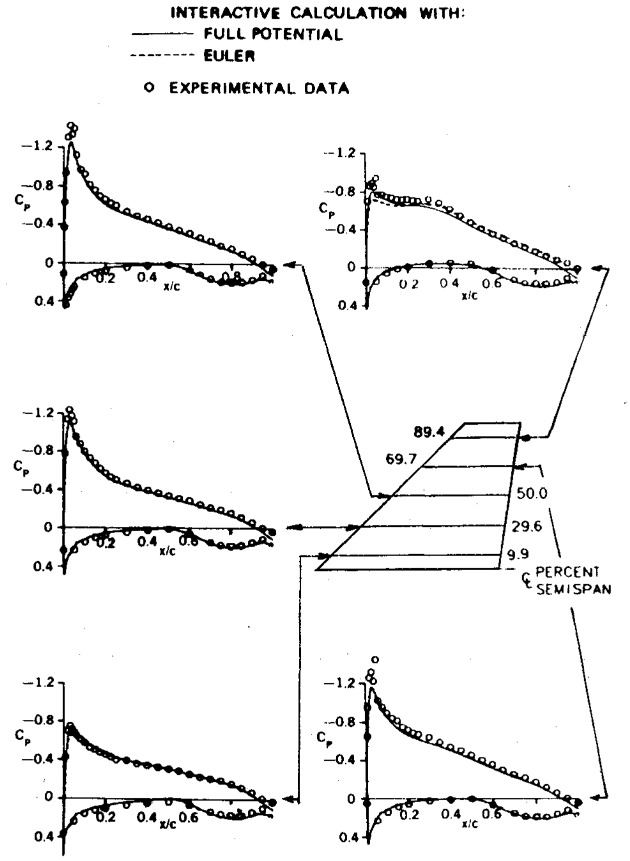

a) Euler with H-grid

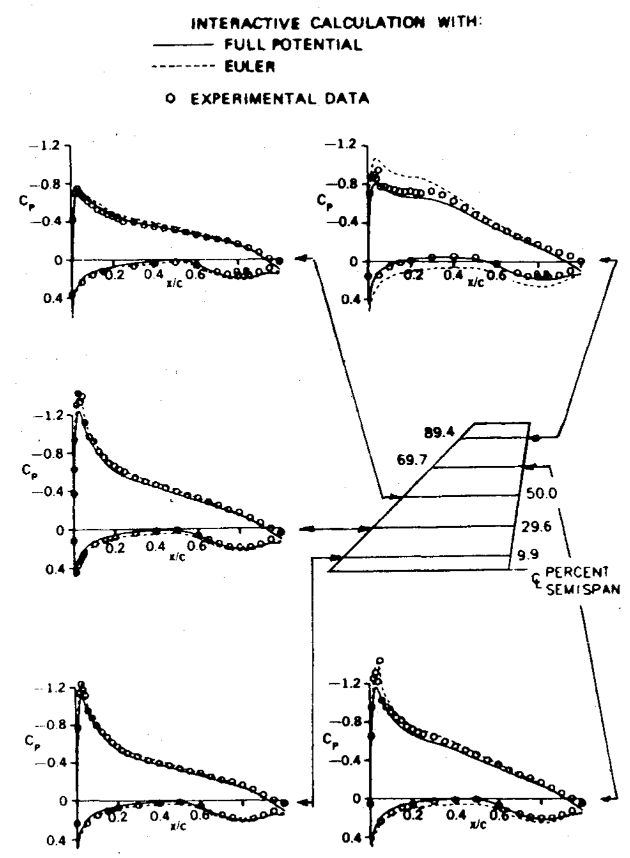

b) Euler with C-grid

Fig. 1 Comparison of calculated and experimental chordwise pressure distributions for $M_\infty = 0.70$, $Re = 6.8 \times 10^6$.

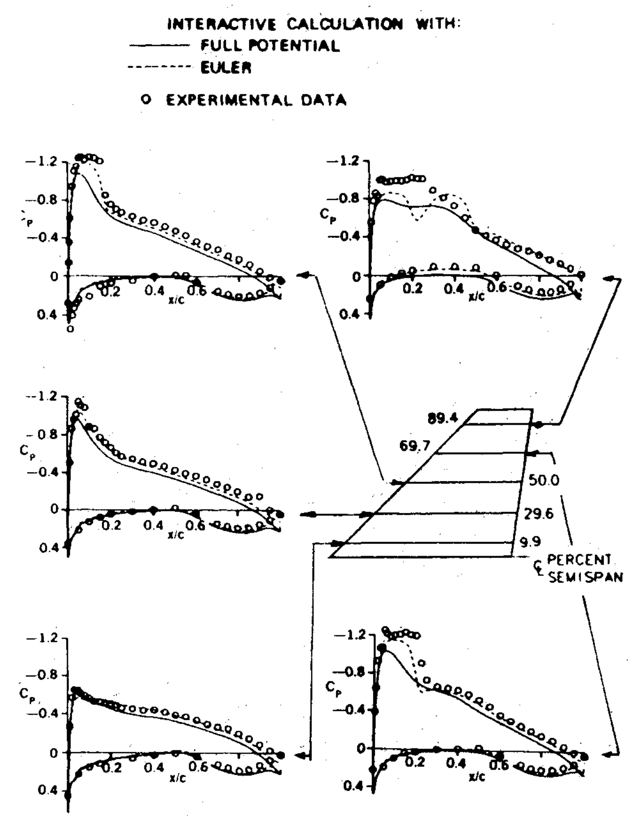

a) Euler with H-grid

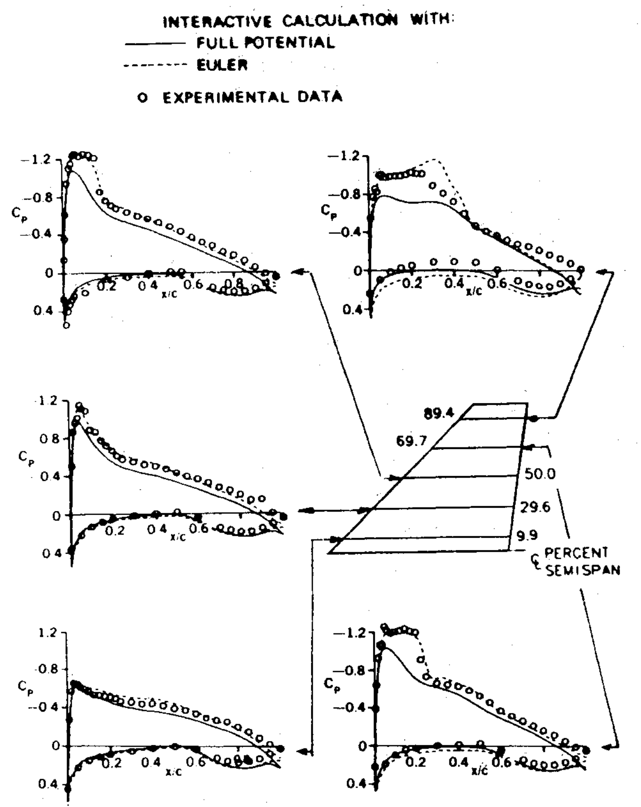

b) Euler with C-grid

Fig. 2 Comparison of calculated and experimental chordwise pressure distributions for $M_\infty = 0.82$, $Re = 6.8 \times 10^6$.

in some details due to differences in the wind tunnels and test conditions. The Ames wind tunnel has a square test section with porous (6% porosity) ceiling and floor, whereas the Lockheed Georgia tunnel has a rectangular test section with variable porosity side walls and ceiling. It was found that in

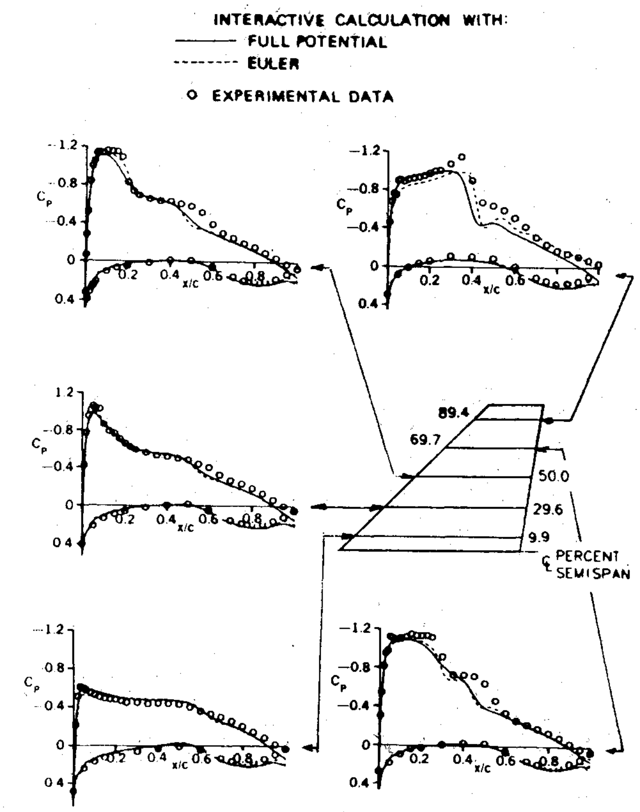

Fig. 3 Comparison of calculated and experimental chordwise pressure distributions for $M_\infty = 0.85$, $Re = 6.8 \times 10^6$.

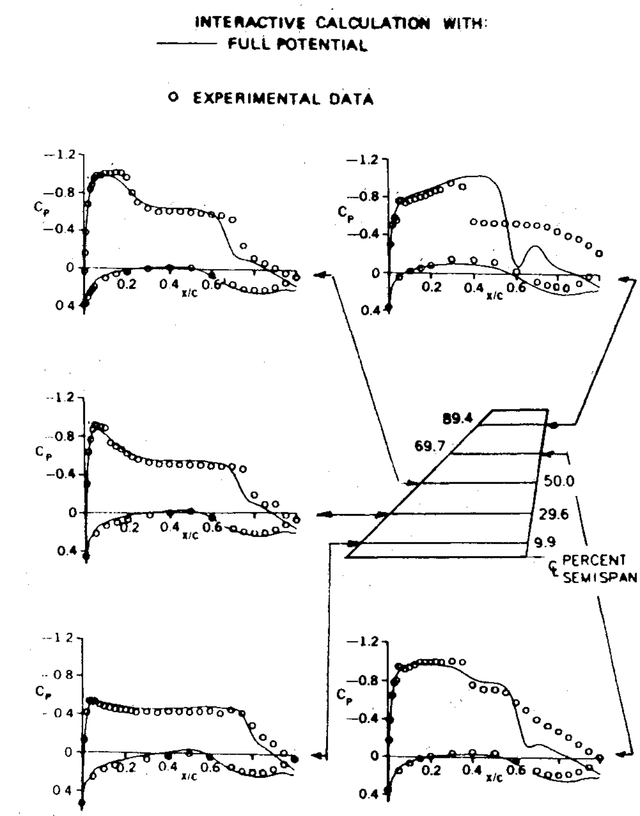

Fig. 4 Comparison of calculated and experimental chordwise pressure distributions for $M_\infty = 0.90$, $Re = 6.8 \times 10^6$.

order to match the calculated and measured pressures near the leading edge, the angle of attack of the smaller model had to be increased to 5.9 deg and a similar check for the larger model indicated negligible lift interference so that the nominal angle of attack was retained.

Concluding Remarks

It is concluded that the interactive calculations with the inviscid flow represented by the Euler code are in better agreement with experimental data than those with the full potential code, especially in the presence of shock waves and with the exception of the wing-tip region. The full potential code gives rise to more diffuse and weaker shocks, which allows calculations at higher Mach numbers without separation. When the flow is not separated, the predicted pressure distributions are in excellent agreement with experimental data. The Euler/thin-layer Navier Stokes (ETLNS) code appears to be better able to evaluate large regions of separated flow.

Acknowledgment

This work was conducted through a joint research project between NASA Ames Research Center and the Douglas Aircraft Independent Research and Development Program.

References

[1]Keener, E. R., "Computational-Experimental Pressure Distributions on a Transonic, Low-Aspect Ratio Wing," AIAA Paper 84-2092, Aug. 1984.

[2]Keener, E. R., "Pressure-Distribution Measurements on a Transonic Low-Aspect Ratio Wing," NASA TM-86683, Sept. 1985.

[3]Chen, L. T., Vassberg, J. C., Chang, K. C., and Cebeci, T., "A Transonic Wing/Body Flowfield Computational Method Using a General Grid Generation Scheme and an Inverse Boundary-Layer Method, Vol. I: Theory," Douglas Aircraft Co., Long Beach, CA, Rept. MDC J3773-1, Jan. 1986.

[4]Chen, L. T., Vassberg, J. C., and Peavey, C. C., "A Transonic Wing-Body Flowfield Calculation with Improved Grid Topology and Shock-Point Generators," *AIAA Journal*, Vol. 23, Dec. 1985, pp. 1877–1884.

[5]Kaynak, U., Holst, T. L., and Cantwell, B. J., "Computation of Transonic Separated Wing Flows Using an Euler/Navier-Stokes Zonal Approach," NASA TM-88311, July 1986 (also "Numerical Simulation of Transonic Separated Flows Over Low-Aspect Wings," *Journal of Aircraft*, Vol. 24, Aug. 1987, pp. 531–539).